Macromolecules

NOTE

pubs.acs.org/Macromolecules

Characterization of Surface Viscoelasticity and Energy Dissipation in a Polymer Film by Atomic Force Microscopy

Dong Wang, Xiao-Bin Liang, Yan-Hui Liu, So Fujinami, Toshio Nishi, and Ken Nakajima*

WPI Advanced Institute for Materials Research, Tohoku University, 2-1-1 Katahira, Aoba, Sendai 980-8577, Japan

Supporting Information

INTRODUCTION

The understanding of properties of polymer surfaces is crucial for the development of new applications in areas such as adhesion, wetting, and friction.[1−6] This effort is hindered, however, by the fact that in most cases it is not appropriate to extrapolate physical parameters of the bulk material as the surface's. Numerous reports have shown that polymeric material near a free surface can have properties which deviate considerably from the bulk.[7−13] Thus, precise quantitative surface mechanical characterizations have been a long-standing academic and technological challenge.

Atomic force microscopy (AFM), particularly the amplitude-modulation dynamic AFM (AM-AFM), is a versatile technique for probing the structure and properties of a wide range of materials with high spatial resolution and capacity to work under various conditions. Recently, AM-AFM has been developed to characterize nanoscale material properties by measuring the phase shift ϕ, arising from the energy dissipated, E_{dis}, during tip−sample interactions

$$E_{dis} = \left(\sin\phi - \frac{\omega}{\omega_0}\frac{A}{A_0}\right)\frac{\pi k A A_0}{Q} \quad (1)$$

in which ω is the excitation frequency, ω_0 is the cantilever's resonance frequency, A is the vibration amplitude during testing, A_0 is the free amplitude without tip−sample interaction, k is the spring constant of cantilever, and Q is the quantity factor.[14−17] By plotting the measured E_{dis} as a function of the A/A_0, a characteristic energy dissipation curve can be obtained. A few reports have employed this technique to characterize surface properties of materials.[1,15,18,19]

Force volume (FV) imaging, an extension of contact mode AFM (static AFM), is another extensively used technique. FV combines topographic imaging and force measurement and can collect simultaneously topography and two-dimensional array of force−distance curves over a specified area. From the force−distance curves, surface properties such as local surface adhesion,[20,21] friction,[22,23] or surface stiffness[24−32] can be deduced based on contact mechanics models such as Hertz or Johnson−Kendall−Robert (JKR). In our previous work,[33,34] by combining FV imaging with JKR[35] contact mechanics to interpret force curves, a nanomechanical mapping technique has been developed. We have shown the true surface topography and investigated the effect of composition on surface morphology and nanomechanical properties of poly(styrene-*b*-ethylene-*co*-butylene-*b*-styrene) (SEBS) triblock copolymer.

In the present study, we extend our method (static AFM measurements) to map the surface viscoelasticity and energy dissipated (E_{dis}) during tip−sample interaction. For comparison, energy dissipation measurement with AM-AFM was also performed. The SEBS consisting of hard PS and soft PEB components was selected because it enables us to get a ratio of $E_{dis}^{PEB}/E_{dis}^{PS}$, in which the E_{dis}^{PEB} and E_{dis}^{PS} are measured with the two different methods. Thus, some unknown factors such as contact area and tip geometry that affect the E_{dis} values can be distinguished by comparing the ratio of $E_{dis}^{PEB}/E_{dis}^{PS}$.

EXPERIMENTAL SECTION

Materials. The poly(styrene-*b*-ethylene-*co*-butylene-*b*-styrene) (SEBS) triblock copolymer was provided by Asahi KASEI Corp. and used without further treatment. The number-average molecular weight, M_n, is 74 000, and the molecular weight distribution, M_w/M_n, is about 1.1. The weight fraction of PS for this triblock copolymer is 42%. Film samples with thickness about 10 μm were prepared by solvent-casting a 4 mg/mL SEBS toluene solution at ambient conditions onto cleaned glass slides. The as-prepared films were first dried in a fume hood for 3 days and then in vacuum at room temperature for another 7 days to remove residual solvent.

AFM Measurements. All AFM measurements were carried out on a commercial Veeco MultiMode system with a NanoScope V controller under ambient conditions. In dynamic AFM, we used silicon cantilevers with resonance frequencies $\omega_0 \sim 300$ kHz and nominal spring constant of k 20−40 N/m (Veecoprobes). Actual spring constant was measured by the thermal tune method. The cantilever's free amplitude A_0 was obtained by measuring amplitude−distance curves on a sapphire sample. The quality factor Q was calculated by dividing the resonant frequency by the width of the resonant peak at half the maximum power.[36] The tip topography, before and after imaging, was checked by tapping mode imaging of a Nioprobe tip-check sample (Aurora NanoDevices Inc., BC, Canada). The commercial SPIP software (Image Metrology A/S, Lyngby, Denmark) was used to obtain the tip radius. The dissipated energy E_{dis} was calculated with eq 1. Experimental details about this method can be found elsewhere.[15,18] In static AFM, measurements were performed using the FV mode on the same AFM. The samples were scanned at constant force using a triangular Si_3N_4 cantilevers with nominal spring constant of 0.32 N/m. Force−distance curves were collected over randomly selected surfaces 1 μm × 1 μm in area at a

Received: May 19, 2011
Revised: September 22, 2011
Published: October 14, 2011

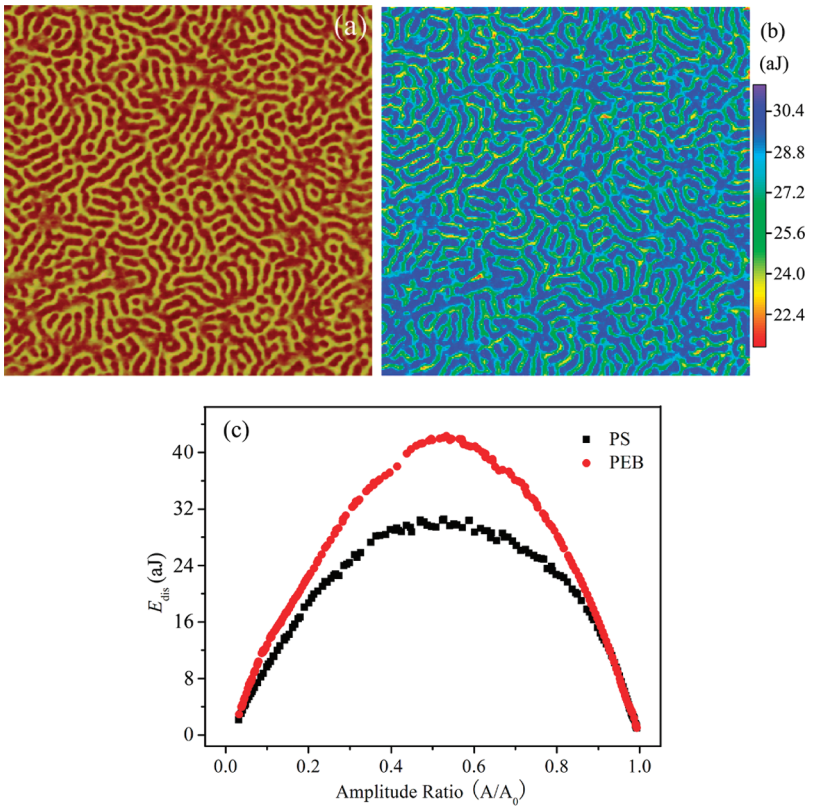

Figure 1. (a) AFM phase image of SEBS film sample. The image was measured with the amplitude ratio $A/A_0 \sim 0.8$. (b) Energy dissipation map converted according to eq 1. Note the scan size is 1 μm. (c) Energy dissipation curve measured as a function of amplitude ratio A/A_0.

resolution of 128 × 128 pixels. The obtained force curves were analyzed using JKR contact mechanics.

RESULTS AND DISCUSSION

The AFM phase image of SEBS film is shown in Figure 1a. As expected, the well-ordered lamellar morphology consisting of bright and dark nanophasic domains can be clearly observed. However, the phase data alone provide little information about the chemical and mechanical heterogeneity of the SEBS film. Without further analysis, identification of the bright or dark regions is usually difficult.[37,38] Several studies have assigned the brighter contrast to the stiffer material and the darker contrast to the softer material,[39−41] but some others report opposite observations.[38,42]

According to eq 1, the AFM phase image can be converted to energy dissipation map (Figure 1b) which enables us to directly link the morphology and mechanical properties of the components. In the E_{dis} image, the blue areas with higher dissipated energy are considered to be the soft PEB blocks, while the blue and green areas with lower dissipated energy are considered to be the hard PS blocks. The typical E_{dis} vs A/A_0 curves corresponding to the PEB and PS components are shown in Figure 1c. According to Garcia,[15] the E_{dis} vs A/A_0 curves suggest that the viscoelastic force dominate the dissipation process between the AFM tip and sample. As can be seen, the dissipated energy of the PEB and PS is considerably different despite that the curve shape and the maximum are dependent on how close the AFM tip is located to the center of the components during the measurements. Locating tip at the center of PS block yields lower maximum and larger difference from that on the PEB regions.

The statistic distribution of the E_{dis} can be perfectly fitted by Gaussian curves (Figure 2a), and we evaluate the average dissipated energy at different amplitude ratio A/A_0. E_{dis} is plotted as a function of the cantilever's oscillation amplitude A/A_0. As shown in Figure 2b, at $A/A_0 \sim 0.55$, the maximum E_{dis} for the PEB and PS are ∼41.0 and ∼33.2 aJ, respectively. Irrespective of the variation of E_{dis} with A/A_0, the $E_{dis}^{PEB}/E_{dis}^{PS}$ ratio remains to be constant value of $\sim 1.2 \pm 0.04$ (the inset in Figure 2b), and the average of difference in energy dissipation is estimated to be 3.3%. Please note that the Figure 1c is the typical E_{dis} vs A/A_0 curves for the PEB and PS components while the Figure 2b is (the statistic average of E_{dis}) vs A/A_0 curves. Thus, they show similar features.

Next, we measured the energy dissipation by FV mode (static AFM). Figures 3a and 3b show typical cantilever deflection curves corresponding to the PEB and PS components, respectively. The force is deduced by multiplying the cantilever's deflection by its spring constant. Generally, the attractive force between tip and sample shows similar feature. But it is larger on PEB regions than that on PS because PEB is more adhesive compared with PS.[34] In the repulsive force regime, the loading−unloading curves overlap, suggesting that the repulsive tip−sample interaction is managed by elastic property of the sample (the elastic modulus of the tip is much higher than that of the PEB and PS). These characteristic of the force curves indicate that the tip−sample interactions are dominated by long-range attractive forces without mechanical instabilities of cantilever and large-scale plastic deformation of sample.[43]

The large difference between loading and unloading force curves are found in the region dominated by attractive forces.[43] It indicates that the energy loss mainly originates from the adhesive

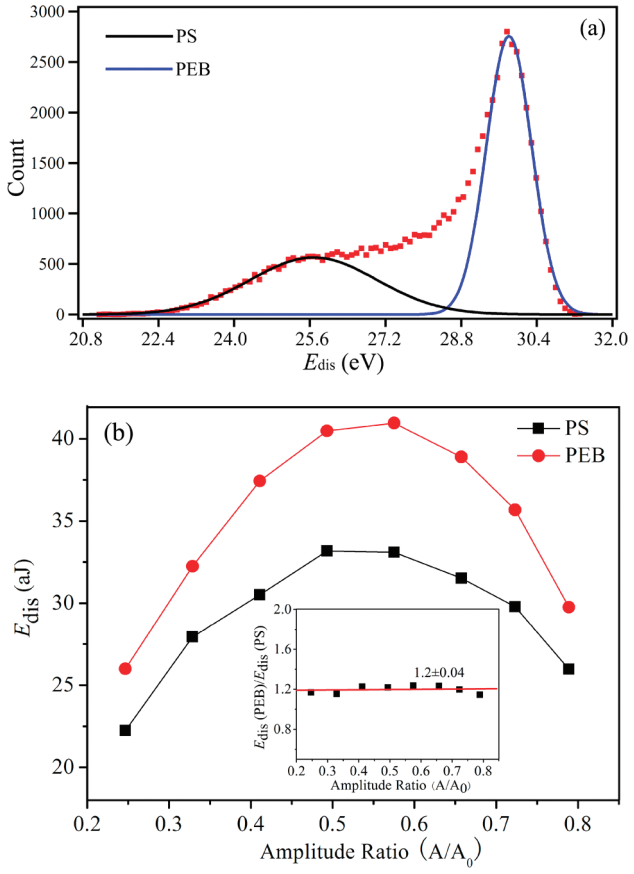

Figure 2. (a) Distribution of energy dissipation. The black and blue solid lines are the Gaussian fit of the experimental data points. (b) Statistic average energy dissipation as a function of the cantilever's oscillation amplitude A/A_0. The inset shows the variation of $E_{dis}^{PEB}/E_{dis}^{PS}$ with the amplitude ratio A/A_0. The average difference in the energy dissipation is estimated to be 3.3%.

forces between tip and specimen. The force for pull-out of polymer chains and/or capillary force also contribute to the dissipated energy.[44] E_{dis} can be deduced by calculating the area enclosed by the force curves.[43] Therefore, based on the 2D array of the force−distance curves, an energy dissipation map can be obtained as shown in Figure 4a. The regions exhibiting larger E_{dis} can be identified as the soft PEB blocks, while the regions showing smaller E_{dis} correspond to the hard PS blocks.

The difference in energy dissipation can be seen in the profile presented in Figure 4b, with $E_{dis}^{PEB} = 42.5 \pm 6.9$ aJ and $E_{dis}^{PS} = 31.8 \pm 2.4$ aJ. The ratio of $E_{dis}^{PEB}/E_{dis}^{PS}$ is calculated to be ~1.3. In FV mode, the trigger threshold is about 0.5 nN, corresponding to an amplitude ratio $A/A_0 \sim 0.8$ in AM-AFM. (The tapping force is calculated to be ~0.5 nN at A/A_0 ~0.8 according to the equation $F = k(A_0^2 - A^2)/2AQ$,[45] and the contact pressure is much lower than the yield strength of the soft PEB.) E_{dis} measured with AM-AFM at $A/A_0 \sim 0.8$ is 29.8 aJ for the PEB and 25.6 aJ for the PS. Although E_{dis} is lower in AM-AFM due to unknown contact area and scan speed,[46,47] the $E_{dis}^{PEB}/E_{dis}^{PS}$ ratio ~1.2 is almost equal to that from FV measurements (~1.3). The consistent $E_{dis}^{PEB}/E_{dis}^{PS}$ ratio suggests that characterization of the E_{dis} by static AFM is quantitatively comparable with that by dynamic AFM.

It is noted that the measured E_{dis} by either static or dynamic AFM are basically qualitative and includes all tip−surface interactions

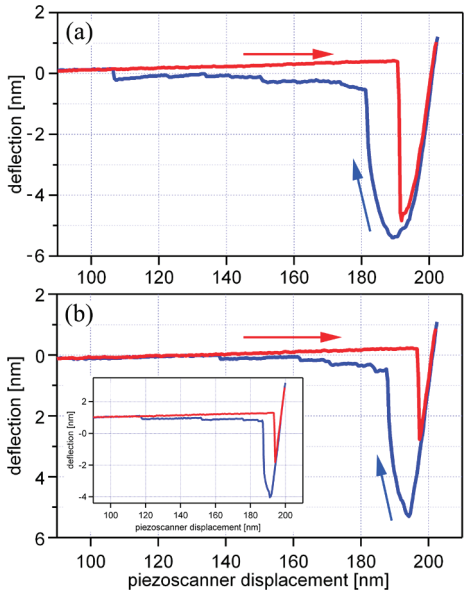

Figure 3. Cantilever deflection−distance curves on (a) PEB and (b) PS region. The arrows indicate the direction of the relative tip−sample displacement. The area enclosed between loading−unloading curves is the dissipated energy. The inset shows the cantilever deflection−distance curve measured on a homo-PS film.

such as viscoelasticity and adhesive energy. In order to distinguish the contribution of viscoelastic and adhesive, we fit the force−deformation curves with the JKR model.[35] The JKR model considers the elastic contact in the presence of adhesion and is described as follows:

$$a^3 = \frac{R}{K}(F + 3\pi wR + \sqrt{6\pi wRF + (3\pi wR)^2}) \quad (2)$$

$$\delta = \frac{a^2}{3R} + \frac{2F}{3aK} \quad (3)$$

where α is the contact radius, R is the radius of curvature for the probe tip, w is the adhesive energy, K is the elastic coefficient, and F is the applied force. The curve fittings are also displayed in Figure 5. As shown in Figure 5b, the JKR fitting to the unloading process is rather well for PS component, indicating that PS behaves in nearly pure elastic manner, consistent with its elastic nature. However, fitting for PEB results in significant deviation, as can be seen Figure 5a. It is known that the JKR theory is derived for perfectly elastic solids and assumes reversible behavior in loading and unloading process. Here, the viscoelasticity of the PEB components plays an important role during unloading process which results in large deviation occurred. Then, the area enclosed by the force−deformation and JKR fitting curves represents the contribution of viscoelastic behavior to E_{dis}, which is 4.5 ± 9.6 aJ for the PEB and 0.55 ± 0.12 aJ for the PS components. The ratio of viscoelasticity induced E_{dis} for the two components is about 8.2, nearly 1 order of magnitude higher than that obtained by calculating the total E_{dis} (the ratio of E_{dis}^{PEB} to E_{dis}^{PS} is ~1.2 and 1.3 in dynamic and static AFM, respectively). This suggests that the imaging contrast can be significantly enhanced. Although E_{dis} is dependent on experimental parameters, the two chemical blocks of the SEBS copolymer can be unambiguously identified as shown in Figure 6. It should be

dx.doi.org/10.1021/ma201148f |*Macromolecules* 2011, 44, 8693–8697

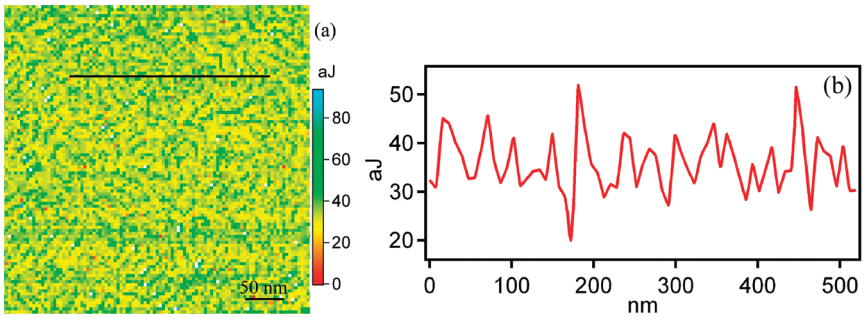

Figure 4. (a) Map of the dissipated energy of SEBS sample calculated from the loading−unloading curves. (b) Numerical values across the section indicated by the line in (a).

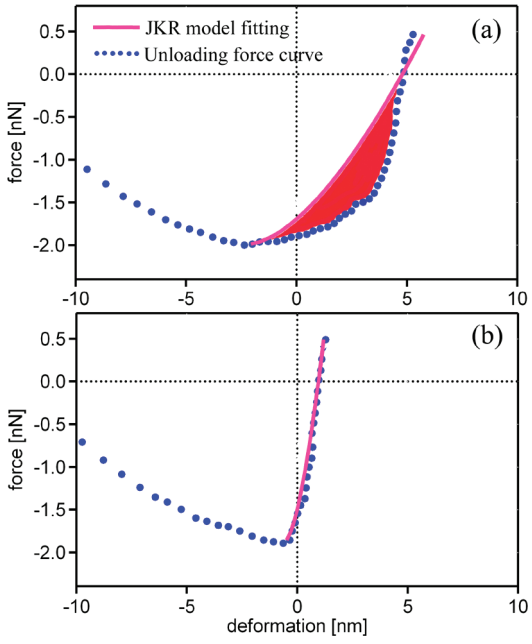

Figure 5. Force−deformation curves of (a) PEB and (b) PS regions. The curve-fitting against JKR contact is superimposed on each curve. The area enclosed by the force−deformation and JKR fitting curve represent the contribution of viscoelasticity to E_{dis}, as shown in (a).

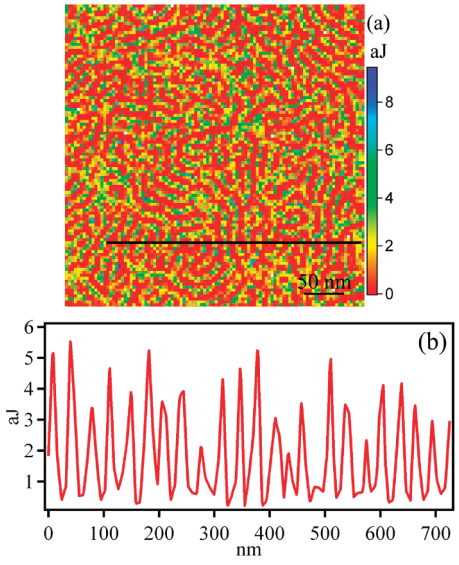

Figure 6. (a) Map of viscoelastic property of the SEBS sample. (b) Numerical values across the section indicated by the line in (a).

noted that Sohn et al. and Knoll et al. have reported that there is an about 10 nm thick layer of the soft component in SEBS and SBS surface.[48,49] However, in the present work, we did not observe such a soft PEB layer in topmost surface of SEBS. As shown in inset in Figure 3, the cantilever deflection−distance curve measured on a homo-PS film (∼10 μm thickness) is similar to the curve measured on the PS component in SEBS (Figure 3b). Moreover, X-ray photoelectron spectroscopy (XPS) results shown in Figure 1S (detailed XPS experiments and results are presented in the Supporting Information) indicate that both phenyl carbon (binding energy 291.7 eV) and hydrocarbon (binding energy 285 eV) are observed on the film surface of the SEBS and the SEBS surface after top layer was removed. And, comparing with the relative intensity of C_{1s} at binding energy of 291.7 eV of the SEBS film surface, there is not evident increase for the SEBS sample after top layer was removed. Therefore, both static AFM profile for homo-PS film and XPS results indicate that the film surface is not covered by soft PEB layer. The volume fraction of PS in SEBS in Sohn's work and SBS in Knoll's work is 13% and 26%, respectively. The SEBS used in our work has a volume fraction of PS ∼39% (weight ratio is 42%). And during the film preparation process, we did not anneal the film sample. The difference in PS/PEB composition and film preparation procedure may cause different surface microstructure than those prepared by annealing process.

It is well-known the viscoelastic property is highly dependent on the frequency (in present study, tip velocity). Thus, further experiments are needed in order to understand the validity of this approximate procedure for measuring the viscoelastic dissipation.

CONCLUSIONS

In summary, we have measured the surface viscoelasticity and dissipated energy E_{dis} between an AFM tip and a surface of the SEBS triblock copolymer with dynamic and static AFM. With dynamic AFM, the measured E_{dis} as a function of the oscillation amplitude shows characteristic shapes for the PEB and PS components. In the A/A_0 range of 0.25−0.80, E_{dis} varies from ∼25.9 to ∼41.0 aJ for the PEB and ∼22.2 to ∼33.2 aJ for the PS, respectively. With FV mode (static AFM), the measured E_{dis} is 42.5 ± 6.9 aJ for the PEB and 31.8 ± 2.4 aJ for the PS components, respectively. Although the measured E_{dis} is dependent on the experimental parameters, such as contact area and tip

geometry, the $E_{dis}^{PEB}/E_{dis}^{PS}$ gives nearly identical ratio (with static AFM, the ratio is 1.3; while with dynamic AFM, it is 1.2). This agreement indicates characterization of the E_{dis} by static AFM is quantitatively comparable with that by dynamic AFM.

On the other hand, the measured E_{dis} by both the static and dynamic AFM, which is determined by the interplay between viscoelastic and adhesive properties of the sample, includes all tip−surface interactions. By analyzing the force−deformation curves together with JKR contact mechanics model, the contribution of viscoelasticity to the total E_{dis} is extracted, and the imaging contrast can be enhanced by nearly 1 order of magnitude. The results show that characterization of the surface viscoelasticity and dissipated energy is a sensitive probe for the detection of local surface mechanical properties of polymeric materials. This provides a rational route for studying the surface mechanical properties in a large of heterogeneous polymeric materials.

■ ASSOCIATED CONTENT

Supporting Information. Experimental details. This material is available free of charge via the Internet at http://pubs.acs.org.

■ AUTHOR INFORMATION

Corresponding Author
*E-mail: knakaji@wpi-aimr.tohoku.ac.jp. Tel: 81-22-2175927.

■ ACKNOWLEDGMENT

The authors thank Dr. A. Muramatsu, Dr. M. Nakaya, and Mr. N. Yagihashi for use their XPS instrument and helpful discussions. The authors also thank Dr. Kazuya Nagata in Asahi Kasei Chemicals Corp. for technical assistance.

■ REFERENCES

(1) Dietz, C.; Zerson, M.; Riesch, C.; Franke, M.; Magerle, R. *Macromolecules* **2008**, *41*, 9259–66.
(2) Gourianova, S.; Willenbacher, N.; Kutschera, M. *Langmuir* **2005**, *21*, 5429–38.
(3) Netravali, A. N.; Caceres, J. M.; Thompson, M. O.; Renk, T. J. *J. Adhes. Sci. Technol.* **1999**, *13*, 1331–42.
(4) Wang, X. P.; Xiao, X. D.; Tsui, O. K. C. *Macromolecules* **2001**, *34*, 4180–85.
(5) Assender, H.; Bliznyuk, V.; Portyrakis, K. *Science* **2002**, *297*, 973–76.
(6) Granick, S.; Kumar, S. K.; Kramer, E. J.; Russell, T. P.; et al. *J. Polym. Sci., Part B: Polym. Phys.* **2003**, *41*, 2755–93.
(7) Jones, R. A. L.; Richards, R. W. *Polymer at Surface and Interfaces*; Cambridge University Press: Cambridge, 1999; Chapter 2.
(8) Keddie, J. L.; Jones, R. A. L.; Cory, R. A. *Europhys. Lett.* **1994**, *27*, 59–64.
(9) Forrest, J. A.; Dalnoki-Veress, K.; Stevens, J. R.; Dutcher, J. R. *Phys. Rev. Lett.* **1996**, *77*, 2002–5.
(10) Yang, Z. H.; Fujii, Y.; Lee, F. K.; Lam, C. H.; Tsui, O. K. C. *Science* **2010**, *328*, 1676–79.
(11) Fakhraai, Z.; Forrest, J. A. *Science* **2008**, *319*, 600–604.
(12) Kajiyama, T.; Tanaka, K.; Takahara, A. *Macromolecules* **1997**, *30*, 280–85.
(13) Tanaka, K.; Taura, A.; Ge, S. R.; Takahara, A.; Kajiyama, T. *Macromolecules* **1996**, *29*, 3040–42.
(14) Cleveland, J. P.; Anczykowski, B.; Schmid, A. E.; Elings, V. B. *Appl. Phys. Lett.* **1998**, *72*, 2613–15.
(15) García, R.; Gómez, C. J.; Martínez, N. F.; Patil, S.; Dietz, C.; Magerle, R. *Phys. Rev. Lett.* **2006**, *97*, 016103.
(16) García, R.; Magerle, R.; Pérez, R. *Nature Mater.* **2007**, *6*, 405–411.
(17) Klinov, D.; Magonov, S. *Appl. Phys. Lett.* **2004**, *84*, 2697–99.
(18) Liu, Y. H.; Wang, D.; Nakajima, K.; Zhang, W.; Hirata, A.; Nishi, T.; Inoue, A.; Chen, M. W. *Phys. Rev. Lett.* **2011**, *106*, 125504.
(19) Spitzner, E. C.; Riesch., C.; Magerle, R. *ACS Nano* **2011**, *5*, 315–20.
(20) Tsukruk, V. V.; Bliznyuk, V. N. *Langmuir* **1998**, *14*, 446–55.
(21) Vezenov, D. V.; Noy, A.; Ashby, P. *J. Adhes. Sci. Technol.* **2005**, *19*, 313–64.
(22) Carpick, R. W.; Salmeron, M. *Chem. Rev.* **1997**, *97*, 1163–94.
(23) Gauthier, S.; Aimé, J. P.; Bouhacina, T.; Attias, A. J.; Desbat, B. *Langmuir* **1996**, *12*, 5126–37.
(24) Cappella, B.; Dietler, G. *Surf. Sci. Rep.* **1999**, *34*, 1–104.
(25) Song, J.; Tranchida, D.; Vancso, G. J. *Macromolecules* **2008**, *41*, 6757–62.
(26) Sahin, O.; Magonov, S.; Su, C. M.; Quate, C. F.; Solgaard, O. *Nature Nanotechnol.* **2007**, *2*, 507–14.
(27) Sahin, O.; Erina, N. *Nanotechnology* **2008**, *19*, 445717.
(28) Jesse, S.; Kalinin, S. V.; Proksch, R.; Baddorf, A. P.; Rodriguez, B. J. *Nanotechnology* **2007**, *18*, 435503.
(29) Stan, G.; Cook, R. F. *Nanotechnology* **2008**, *19*, 235701.
(30) Tsukruk, V. V.; Sidorenko, A.; Gorbunov, V. V.; Chizhik, S. A. *Langmuir* **2001**, *17*, 6715–19.
(31) Ebenstein, D. M.; Wahl, K. J. *J. Colloid Interface Sci.* **2006**, *298*, 652–62.
(32) Ahn, D. C.; Shull, K. R. *Macromolecules* **1996**, *29*, 4381–90.
(33) Wang, D.; Fujinami, S.; Nakajima, K.; Nishi, T. *Macromolecules* **2010**, *43*, 3169–72.
(34) Wang, D.; Fujinami, S.; Liu, H.; Nakajima, K.; Nishi, T. *Macromolecules* **2010**, *43*, 9049–55.
(35) Johnson, K. L.; Kendall, K.; Roberts, A. D. *Proc. R. Soc. London, Ser. A* **1971**, *324*, 301–13.
(36) Chapter 9 Q Control in "Veeco Nanoscope V Controller Manual-E" (004-992-000).
(37) Raghavan, D.; Gu, X.; Nguyen, T.; VanLandingham, M. R.; Karim, A. *Macromolecules* **2000**, *33*, 2573–83.
(38) Bar, G.; Thomann, Y.; Brandsch, R.; Cantow, H. J.; Whangho, M. H. *Langmuir* **1997**, *13*, 3807–12.
(39) Bar, G.; Thomann, Y.; Brandsch, R.; Whangbo, M. H. *Langmuir* **1998**, *14*, 1219–26.
(40) Sauer, B. B.; McLean, R. S.; Thomas, R. R. *Langmuir* **1998**, *14*, 3045–51.
(41) Magonov, S. N.; Elings, V.; Papkov, V. S. *Polymer* **1997**, *38*, 297–307.
(42) Magonov, S. N.; Ellings, V.; Whangbo, M. H. *Surf. Sci.* **1997**, *375*, L385–L391.
(43) Tamayo, J.; García, R. *Appl. Phys. Lett.* **1998**, *73*, 2926–28.
(44) Nakajima, K.; Yamaguchi, H.; Lee, J. C.; Kageshima, M.; Ikehara, T.; Nishi, T. *Jpn. J. Appl. Phys.* **1997**, *36*, 3850–54.
(45) Sugawara, Y. In *Atomic Force Microscopy*; Morita, S., Ed.; Roadmap of Scanning Probe Microscopy; Springer: Berlin, 2006; p 16.
(46) Bar, G.; Delineau, L.; Brandsch, R.; Bruch, M.; Whangbo, M. H. *Appl. Phys. Lett.* **1999**, *75*, 4198–4200.
(47) Tamayo, J.; García, R. *Appl. Phys. Lett.* **1997**, *75*, 2394–97.
(48) Knoll, A.; Magerle, R.; Krausch, G. *J. Chem. Phys.* **2004**, *120*, 1105–16.
(49) Sohn, K. E.; Kojio, K.; Berry, B. C.; Karim, A.; Coffin, R. C.; Bazan, G. C.; Kramer, E. J.; Sprung, M.; Wang, J. *Macromolecules* **2010**, *43*, 3406–14.